Geodesic Active Contours with Adaptive Configuration for Cerebral Vessel and Aneurysm Segmentation

Xin Yang, K.T.Tim Cheng
Dept. of Electrical and Computer Engineering
University of California, Santa Barbara
Santa Barbara, CA, USA
xinyang@umail.ucsb.edu, timcheng@ece.ucsb.edu

Aichi Chien
Division of Interventional Neuroradiology
University of California, Los Angeles Medical School
Los Angeles, CA, USA
aichi@ucla.edu

***Abstract*— Active contour is a popular technique for vascular segmentation. However, existing active contour segmentation methods require users to set values for various parameters, which requires insights to the method's mathematical formulation. Manual tuning of these parameters to optimize segmentation results is laborious for clinicians who often lack in-depth knowledge of the segmentation algorithms. Moreover, a global parameter setting applied to all voxels of an input image can hardly achieve optimized results due to vessels' high appearance variability caused by the contrast agent inhomogeneity and noises. In this paper, we present a method which adaptively configures parameters for Geodesic Active Contours (GAC). The proposed method leverages shape filtering to produce a parameter image, each voxel of which is used to set parameters of GAC for the corresponding voxel of an input image. An iterative process is further developed to improve the accuracy of the shape-based parameter image. An evaluation study over 8 clinical datasets demonstrates that our method achieves greater segmentation accuracy than two popular active contour methods with manually optimized parameters.**

Keywords—Cerebral vessel, Aneurysm, Adaptive configuration, Geodesic active contour, Shape analysis

I. INTRODUCTION

A cerebral aneurysm is an abnormal enlargement of any artery located at or near bifurcations of the arteries in the Circle of Willis. Aneurysm rupture accompanied with subarachnoid hemorrhage (SAH) is a serious complication which causes 32% to 67% fatality and 10.9% morbidity due to intracranial bruise, subsequent recurrent bleeding, stroke, hydrocephaly and vessel spasm [1][2].

Computed Tomography Angiograph (CTA) is one of the most frequently used diagnostic images for vessel examination and aneurysm detection. The segmentation of aneurysm and the surrounding vascular structure on CTA images has a significant role in diagnosis and treatment planning. Despite the tremendous amount of dedicated research, automatic vascular segmentation on CTA images remains challenging due to noises, inhomogenous image intensity and gradient, and the presence of bone tissues which are close to vessels and have similar intensity values as vessels.

Active contour within the level set framework [6][9][11][13] has been widely accepted as a suitable technique for vascular segmentation due to its ability to handle topology changes and adapt to shape of complex structures such as blood vessels. However, the outcome of active contour segmentation depends on a number of parameters. Finding the right set of parameters can be difficult even for users familiar with the algorithm. Besides, vessels usually present high appearance variability due to the contrast agent inhomogeneity, noises and image artifacts. As a result, a global parameter configuration for all voxels of an image can hardly achieve satisfactory results. Fig. 1 shows exemplar segmentation results based on two configurations. Configuration A can suppress noises on slice ①, while causes discontinued boundary on slice ②, and in turn causes leakage as indicated in ③. Configuration B enhances gradients to ensure a closed boundary on slice ② while increases noises within the vessel on slice ①, yielding an incomplete segmentation. Difficulties in parameter selection greatly discourage the use of active contour techniques in the clinical environment. An adaptive and location-dependent configuration method is of high demand to bridge the gap between algorithm advancement and clinical routine, while insufficient effort has been made in this direction.

In this paper we focus on adaptive parameter setting for Geodesic Active Contours (GAC) [4], a widely-used active contour method relying on gradient information for contour evolution. A key parameter of GAC that critically affects the final segmentation results and is sensitive to image content lies in the step of gradient mapping. The key idea of our method is to utilize shape information as prior knowledge to guide parameter setting in this step. Specifically, we construct a *parameter image*, each voxel of which is determined by shape filtering and is used to configure the mapping function for the corresponding voxel of an input image. The result of shape

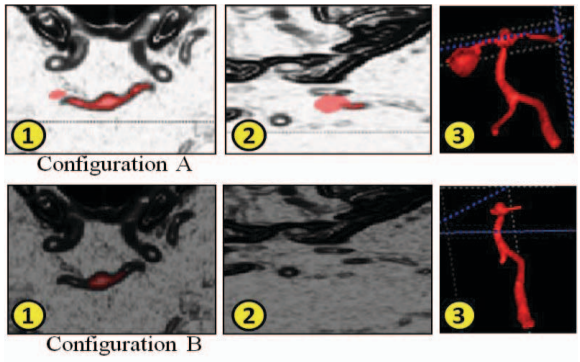

Fig. 1. Segmentation results obtained by two global configurations of Geodesic Active Contours (GAC). The first and second rows show the results produced by Configurations A and B respectively. For each configuration, ① and ② display the feature maps of two generated slices, and ③ shows the segmentation result. Red color indicates segmented voxels.

1051-4651/14 $31.00 © 2014 IEEE
DOI 10.1109/ICPR.2014.553

filtering inevitably contains noises which result in errors in the parameter image and in turn mislead the configuration of GAC. To address this problem, we propose to iteratively correct the shape-based parameter image using the result of gradient mapping since it provides complementary information to the shape and thus is less likely to have errors at the same location.

An evaluation study over 8 clinical datasets demonstrates that our method achieves 86.1-99.2% segmentation accuracy with respect to the ground-truth. Compared to two widely-used active contour methods (i.e. geodesic active contours [4] and region completion [5]) with manual performance optimization our method can achieve consistently greater segmentation accuracy in addition to significant reduction in the configuration effort.

The rest of the paper is organized as follows: Section 2 reviews the related work. Section 3 presents details of the proposed method. In Section 4, we compare performance of our method with related active contour methods. Section 5 concludes the paper.

II. Related Work

In recent years, active contour implemented using level set techniques has been widely used for object segmentation. A number of active contour segmentation methods have been developed to date [4][5][10][12][14]. However, general active contour methods can hardly achieve satisfactory performance for 3D vascular segmentation due to the complex structure of vessels, limited image resolution, and artifacts in medical imagery. Several efforts have been made to adapt existing active contour methods to 3D vascular segmentation by leveraging specific characteristics (i.e. hyper-intensity and tubular-like shapes) of vessels. Nain et al. [6] proposed a ball measurement which is used as a shape prior to penalize local widening of contours and to maintain the shape elongation. However, their method may incorrectly penalize local enlargement due to aneurysms and bifurcations, resulting in incomplete segmentation at those locations. Several vessel-dedicated features are designed to produce a force field which drives the contours towards vessel edges. Notable results include the spherical flux measure [15], optimally oriented flux [16][17], the Hessian-based vessel filter [8], etc. Recently, Hernandez et al. proposed non-parametric geodesic active contours [9] which incorporate high-order multiscale features to model cerebral vessel and aneurysm tissues. Despite of performance improvements demonstrated by these methods dedicated to 3D vascular segmentation, setting proper values for a set of parameters to achieve optimized results remains a problem for users.

To bring active contour segmentation to the fingertips of general users, Yushkevich et al. [3] developed ITK-SNAP, an open-source software which utilizes user-friendly interface and live feedback to facilitate parameter selection for medical image segmentation. However, their method still requires manual configuration. Another limitation is that the software only allows a single configuration that globally applied to all voxels in the entire 3D image, which often results in sub-optimal performance.

III. Our Method

In this section, we begin with a brief introduction of Geodesic Active Contours followed by details of the proposed method for adaptive parameter setting.

A. Geodesic Active Contours

Active contour segmentation constitutes a popular class of image segmentation techniques that evolve a closed curve/surface through a combination of different forces: *external* forces, derived from the image, and *internal* forces, derived from the contour's geometry and are used to impose regularity constraints on the shape of the contour. GAC defines forces acting on the contour as:

$$F = \alpha g_I + \beta\kappa + \gamma(\nabla g_I \cdot \vec{N}), \tag{2}$$

where g_I is the speed function derived from the gradient magnitude of the input image I and acts outward to drive the contour to expand; κ is the mean curvature of the contour which controls the smoothness of the evolving curve; $\vec{N}$ is the unit normal to the contour and $\nabla g_I \cdot \vec{N}$ is called advection forces which acts inwards when the contour approaches an edge and is parallel to it; α, β and γ are weights modulating the relative contributions of the three components of F.

In [4], the speed function g_I is derived as follows:

$$g_I(x) = \frac{1}{1+(NGM_I(x)/\nu)^2}$$
$$NGM_I(x) = \frac{\| \nabla(G_\sigma * I(x)) \|}{\max_I \| \nabla(G_\sigma * I(x)) \|} \tag{3}$$

where NGM_I is the normalized gradient magnitude of $I(x)$; $G_\sigma * I(x)$ denotes convolution of $I(x)$ with an Gaussian kernel G_σ; ν is a user-specified parameter that determines the shape of the monotonic mapping between a normalized gradient magnitude and a speed function. According to Eq. (3), the value of g_I is close to 0 at edges and closed to 1 in regions where intensity is nearly constant.

Choices of α, β, γ and ν affect the outcome of GAC, but we observe that the value of ν is much more content-dependent than the other three parameters. We evaluate the variances of optimal values for each parameter with respect to different images. Specifically, for 8 different datasets (details of datasets will be provided in Section 4) we exhaustively search optimal parameter values for each dataset and for each parameter we calculate the variance of the 8 optimal values. Experimental results show that optimal values for α, β, γ remain the same for all datasets (i.e. variance is 0) while optimal values of ν vary significantly (i.e. variance is ~30% of the mean). In addition, due to imhomogeneous image gradient on vessel boundaries, a single choice of ν may either lead to a large g_I at the boundary of a vessel which has a small gradient value, yielding leakage (illustrated in the first row of Fig.1) or cause a small g_I inside a vessel tube due to high frequency noises, yielding incomplete segmentation (illustrated in the second row of Fig.1). Therefore, the value of ν should be determined according to image contents and could have different values for different regions, or even voxels. In the following, we present our content-based method for adaptive selection of ν.

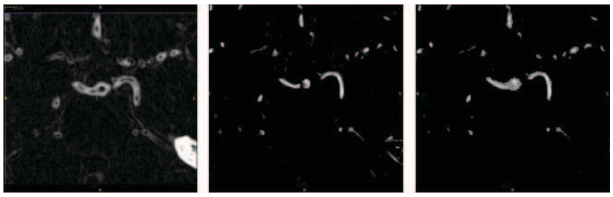

(a) (b) (c)

Fig. 2. Examplar (a) Gradient image of a slice, (b) intial parameter image and (c) the updated parameter image of the slice.

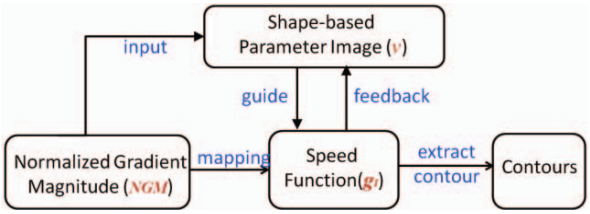

Fig. 3. Workflow of adaptively-configured Geodesic Active Contours.

B. *Adaptive Parameter Setting for Speed Function*

A key characteristic of blood vessels is their specific shapes. The main idea of our method is to utilize shape information as prior knowledge to guide the mapping between gradient and speed function so that gradients at boundaries of vessel-like regions are enhanced while those inside or outside vessel-like regions are suppressed. Specifically, the outcome of our adaptive configuration algorithm is a *parameter image* which is constructed based on shape filtering and each element of a parameter image is used to configure the speed function for the corresponding voxel of an input image.

A number of methods have been developed for vessel-like shape filtering [8][18]. These methods usually use tubes and blobs to model shapes of healthy vessels and aneurysms respectively. Shape filters are designed with the goal of producing large response values at locations close to the centers of tube-/blob-like regions, small values at borders of tube-/blob-like regions and a zero value everywhere else. With the modified speed function as Eq. (4), responses of shape filtering $v(x)$ meet the objective of amplifying gradients at vessel borders, reducing gradients inside vessels, and removing gradients on non-vessel tissues, and thus can be used as our parameter image.

$$g_I(x)=\begin{cases}\dfrac{1}{1+\left(NGM_I(x)/(v(x))\right)^2} & v(x)\neq 0\\ 1 & v(x)=0\end{cases} \tag{4}$$

An error-free shape-based parameter image is hard to achieve, especially at sites where geometric structure of vessels cannot be approximated by pre-defined shape models. For instance, bifurcations of arteries which cannot be modeled using a single tube or a blob may incorrectly result in zero $v(x)$ (as shown around the center of parameter image in Fig. 2(b)) and consequently lead to discontinued contours at these locations. Despite the imperfection of both gradient image and parameter image (Fig. 2(a) and (b)), errors on these two images are caused by different reasons (i.e. low contrast causes discontinuities in a gradient image while inconformity with pre-defined models causes errors in a parameter image), thus they are less likely to occur at the same location. Based on this observation, we propose an iterative process in which the parameter image is iteratively updated by the gradient and the speed g_I, and in turn the mapping between the gradient and the speed is iteratively guided by an updated parameter image.

Fig. 3 illustrates the workflow of our Geodesic Active Contours with adaptive configuration. In the following, we present details of iterative parameter image construction.

Iterative Parameter Image Construction

The key idea of iterative parameter image construction is based on the vessel continuity. The shape responses of a voxel v_i should not be significantly different from that of a connected voxel v_{i-1} if v_{i-1} has been proven to reside in a vessel. We consider v_i is connected with v_{i-1} if v_i is adjacent to v_{i-1} and the gradient magnitude of v_i is close to that of v_{i-1}. We can reliably classify a voxel as a vessel voxel if its speed function value is non-zero, which indicates both a large gradient magnitude and a non-zero shape response according to Eq. (4). We replace the shape response of v_i with the response of its connected voxel v_{i-1} if the response of v_i is much smaller than that of v_{i-1}. Once the parameter image is revised, we update the speed function accordingly. The process iterates until the parameter image become stable. The updated parameter image of Fig. 2(b) is shown in Fig. 2(c). Fig. 4 shows detailed steps of parameter image construction:

- An initial shape-based parameter image is first constructed based on mutiscale Hessian matrix analysis [8]. In particular, two shape filters are employed to enhance tube-like and blob-like regions respectively as:

$$V_t=\begin{cases}0 & if\ \lambda_2>0\ or\ \lambda_3>0\\ \left(1-\exp\left(-\frac{R_A^2}{a^2}\right)\right)\exp\left(-\frac{R_B^2}{b^2}\right)\left(1-\exp\left(-\frac{S_A^2}{c^2}\right)\right) & otherwise\end{cases} \tag{5}$$

$$V_b=\begin{cases}0 & if\ \lambda_1>0\ or\ \lambda_2>0\ or\ \lambda_3>0\\ \left(1-\exp\left(-\frac{S_A^2}{c^2}\right)\right) & otherwise\end{cases} \tag{6}$$

$$R_A=\frac{|\lambda_1|}{\sqrt{|\lambda_2\lambda_3|}},\quad R_B=\frac{|\lambda_2|}{|\lambda_3|},\quad S=\sqrt{\lambda_1^2+\lambda_2^2+\lambda_3^2} \tag{7}$$

where V_t and V_b are tube and blob filters respectively; λ_1, λ_2 and λ_3 are eigenvalues of Hessian matrix and $|\lambda_1|\leq|\lambda_2|\leq|\lambda_3|$; a, b and c are weights modulating the relative contributions of the three components of filters. Each voxel of an initial parameter image is set as the greater value of V_t and V_b at the corresponding location. It is worth noting that although 3 more parameters (i.e. a, b and c) are introduced, like α, β, γ in Eq. (2), they are not sensitive to image content. Thus they can be set statically and do not need to be exposed to end users.

- Connected components (CC) are detected on the initial parameter image. Iterative updates to the parameter image are conducted within each connected component. This scheme is designed to facilitate false positive removal, which will be explained in the following.

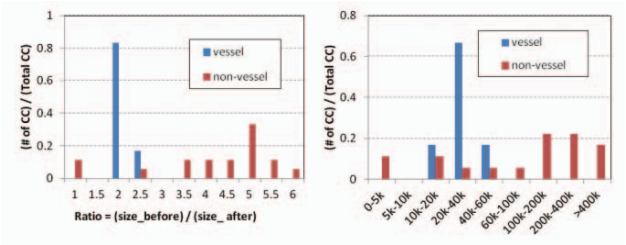

Fig. 5. Distributions of ratio of connected components before and after expansion and size of connected components.

- It's possible that Eqs. (5) and (6) may incorrectly produce non-zero responses to non-vessel tissues, especially on the edges of bones. After parameter image update, the false responses at bone tissues could spread widely, from edges to the entire bone tissues. To distinguish the true responses at vessels and the false responses at non-vessel tissues, we analyze two attributes of each connected component: (1) the ratio of its size before and after the update and (2) the size of each connected component. Statistical analysis over 8 clinical data reveals that the distributions of the two numbers are quite different for vessels and non-vessel tissues (as shown in Fig. 5), thus a simple thresholding strategy can remove most false positives. Specifically, if the size ratio is greater than 2.5 and the size is greater than 60k voxels, the component is unlikely to be a vessel. Note that these threshold values, chosen based on analysis of ground-truth data, do not require manual tuning by users. In principle, the more ground-truth data is analyzed, the greater accuracy the thresholds would be.

IV. Experiential Results

In this section, we provide quantitative evaluation of our method using clinical data. We first describe our datasets and evaluation metric, followed by the results and analysis.

A. Datasets

This study, approved by University of California, Los Angeles institutional review board, consists of evaluation of 8 CTA clinical datasets. Each dataset contains a 3D image volume including both anterior cerebral circulation arteries (ACCA) and posterior cerebral circulation arteries (PCCA). Single aneurysm appears on all datasets, four located at the bifurcation of middle cerebral arteries (MCA) and the other four located at the tip of basilar arteries (BA).

The acquisition of data was performed using 64 detectors scanner with 120 kV/250-300 mA for amplifier tube, 0.75 slice collimation and slice spacing of 0.5 mm. A total of 63 ml of non-ionic contrast fluid was intravenously administrated at a rate of 3 ml/s. The images were reconstructed on a 512x512 volume with a square FOV of 18 cm, yielding an in-plane resolution of 0.35 mm.

B. Evaluation Metric

We evaluate the segmentation accuracy by Dice Similarity Coefficient (DSC), a widely used metric for validation of segmentation algorithms in different medical image modalities [9][13]. DSC is defined as:

$$DSC(S,G)=\frac{2\times|S\cap G|}{|S|+|G|}, \tag{8}$$

where S and G represent segmented voxels and ground-truth voxels respectively; | • | denotes the set cardinality. The ground-truth for evaluation is labeled manually by experts with slice-by-slice delineation of contours. Fig. 7 (a) shows ground-truth of datasets 1, 3, 4 and 5. DSC ranges from 0, if S and G do not overlap, to 1, if S and G are identical.

C. Experimental Setup

We compare our method, adaptively-configured geodesic active contours based on an iteratively-updated parameter image (AGAC-Iterative), with three other methods: region competition (RC) [5], geodesic active contours (GAC) [4] and a simplified version of our method, adaptive-configured GAC based on a parameter image constructed via a single round of shape filtering (AGAC-Single). For RC and GAC, we manually tune parameters to optimize the segmentation results. Specifically, for RC we uniformly choose 8 parameter values ranging from 1200 to 1900 for the upper bound intensity threshold, leading to 8 configurations. For GAC, we set the value of v ranging from 0.016 to 0.044 with a step of 0.004, yielding 8 configurations as well. For all methods, we place 10 seeds (i.e. 10 balloons with a radius of 2.0) as initial contours at the same locations of ACCA and PCCA respectively.

We use ITK-SNAP [3] implementations for GAC and RC. For shape filtering based on multi-scale hessian matrix analysis, our implementation is built upon ITK [19].

D. Results

First, we use two examples to illustrate how sensitive the segmentation accuracy, measured by DSC, to the configurations for the conventional GAC and RC methods. Fig. 6 plots DSC resulting from these 8 different configurations for datasets 1 and 5. For GAC, the segmentation accuracy improves as v increases, until v reaches a certain value. This is because a larger v gives a greater expansion speed of a contour, resulting in a more complete segmentation. After v becomes sufficiently large, increasing v further will adversely degrade the accuracy (i.e. lower DSC). Since an excessively large v can lead to a non-zero speed at vessel edges which have small gradient magnitude values, yielding a leakage. Similar phenomenon was also observed for RC. Although for both datasets similar trends were observed for both RC and GAC, the configuration producing the greatest DSC is dataset- and location-dependent. For example, for ACCA of dataset 1, the best result of GAC is achieved by configuration 4 while for dataset 5 the best result of GAC is produced by configuration 3. When comparing the GAC results of ACCA and PCCA of dataset 1, the greatest DSC is achieved by configurations 4 and 7 for ACCA and PCCA respectively. Similarly, RC's results are dataset- and location-dependent as well. In comparison, our methods, AGAC-Single and AGAC-Iterative, do not require manual tuning of parameters. We therefore indicate their final DSCs in these charts as straight horizontal lines. Clearly our methods outperform RC and GAC for both ACCA and PCCA.

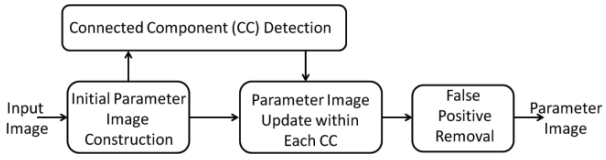

Fig. 4. Workflow of Iterative Parameter Image Construction

Tables 1 and 2 show a complete comparison of the four methods over 8 datasets. The DSC numbers for RC and GAC are based on the results of configurations which produce the most accurate segmentation among all explored configurations. Three observations can be made from these results:

1) For RC and GAC, even the best result, among all explored configurations, fails to provide a satisfactory segmentation. The DSC of RC is only 66.1-80.0% for ACCA and 57.1-89.1% for PCCA. For GAC, the DSC is even lower: 26.6-48.5% for ACCA and 27.1-75.8% for PCCA respectively. In general, the DSC of ACCA is lower than that of PCCA for both RC and GAC. This is mainly because ACCA are surrounded by sphenoid bone which appears closer to ACCA than PCCA. Therefore, leakage to the neighboring bone tissues is more likely to occur at ACCA locations. In addition, the geometric structure of ACCA is more complicated than that of PCCA. Therefore, segmentation of ACCA is more challenging than that of PCCA.

2) Our adaptive methods (single and iterative) consistently achieve superior performance to RC and GAC for all datasets. In addition, with help of the false positive removal process (outlined in Fig. 4), most of the non-vessel tissues are removed, and hence leakage to adjacent bones is effectively prevented.

3) Iterative updates to a parameter image can prevent discontinuities arising from inconformity with pre-defined shape models, and consequently improve segmentation results. By comparing the last two columns of Tables 1 and 2 we observe that AGAC (Iterative) further improves the performance of AGAC (Single) by 4.2-23.2% for ACCA and 2.0-14.2% for PCCA. Fig. 7 (b)~(e) presents four exemplar segmentation results obtained by the four methods.

V. Conclusions

In this paper, we introduce adaptively-configured GAC for segmentation of cerebral vessels and aneurysms. The method adaptively adjusts parameters by leveraging the local shape around an image voxel to guide the mapping between the gradient magnitude of the voxel and the evolution speed of a contour at its location. An iterative process is further introduced to improve the result of local shape analysis. Experimental results over 8 clinical datasets demonstrate that our method outperforms two popular active contour segmentation methods (i.e. region competition and geodesic active contour) with manually optimized parameters.

This work primarily demonstrated the value of the adaptive configuration idea to GAC. However, we believe this idea is also applicable to other active contour methods. Our future work thus includes an adaptive configuration framework for general active contour methods which helps make active contour segmentation more easily useable by end users.

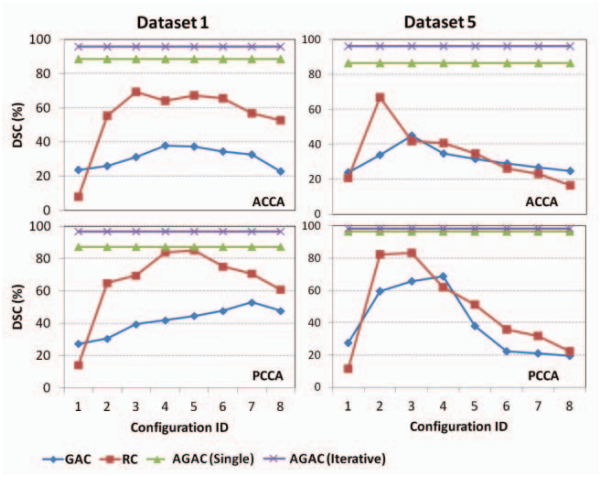

Fig. 6. Segmentation results with respect to different parameter configurations for datasets 1 and 5.

Table 1. DSC of ACCA using Different Methods

Dataset ID	RC	GAC	AGAC (Single)	AGAC (Iterative)
1	69.4	37.3	88.7	95.8
2	66.1	47.7	79.8	86.1
3	71.2	38.2	80.1	98.7
4	69.3	26.6	84.4	94.5
5	66.8	45.0	86.4	96.3
6	80.0	43.7	88.7	92.4
7	79.9	32.0	86.2	98.9
8	70.7	48.5	88.0	96.3

Table 2. DSC of PCCA using Different Methods

Dataset ID	RC	GAC	AGAC (Single)	AGAC (Iterative)
1	85.0	53.0	87.3	96.7
2	57.1	69.0	90.0	94.8
3	89.1	73.4	96.9	99.2
4	70.6	27.1	83.3	95.1
5	83.4	68.8	96.5	98.4
6	78.5	70.0	95.3	97.0
7	70.1	44.1	87.5	96.1
8	84.3	75.8	95.8	96.8

References

[1] Guidelines for the Management of Aneurysmal Subarachnoid Hemorrhage. *Stroke*. 2012 Jun;43(6):1711-37.

[2] J. Huang, J. M. vab Gelder. The Probability of Sudden Death from Rupture of Intracranial Aneurysms: A Meta-Analysis. *J. Neruosurg*. 2002. 51(5), 1101-1105.

[3] P. A. Yushkevich, J. Piven, H. C. Hazlett, R. G. Smith, S. Ho, J. C. Gee, and G. Gerig. User-guided 3D active contour segmentation of anatomical structures: Significantly improved efficiency and reliability. *Neuroimage* 2006 Jul. 1;31(3):1116-28.

[4] V. Caselles, R. Kimmel, G. Sapiro. Geodesic Active Contours. *Int. J. Comput. Vis*. 1997. 22, 61-79.

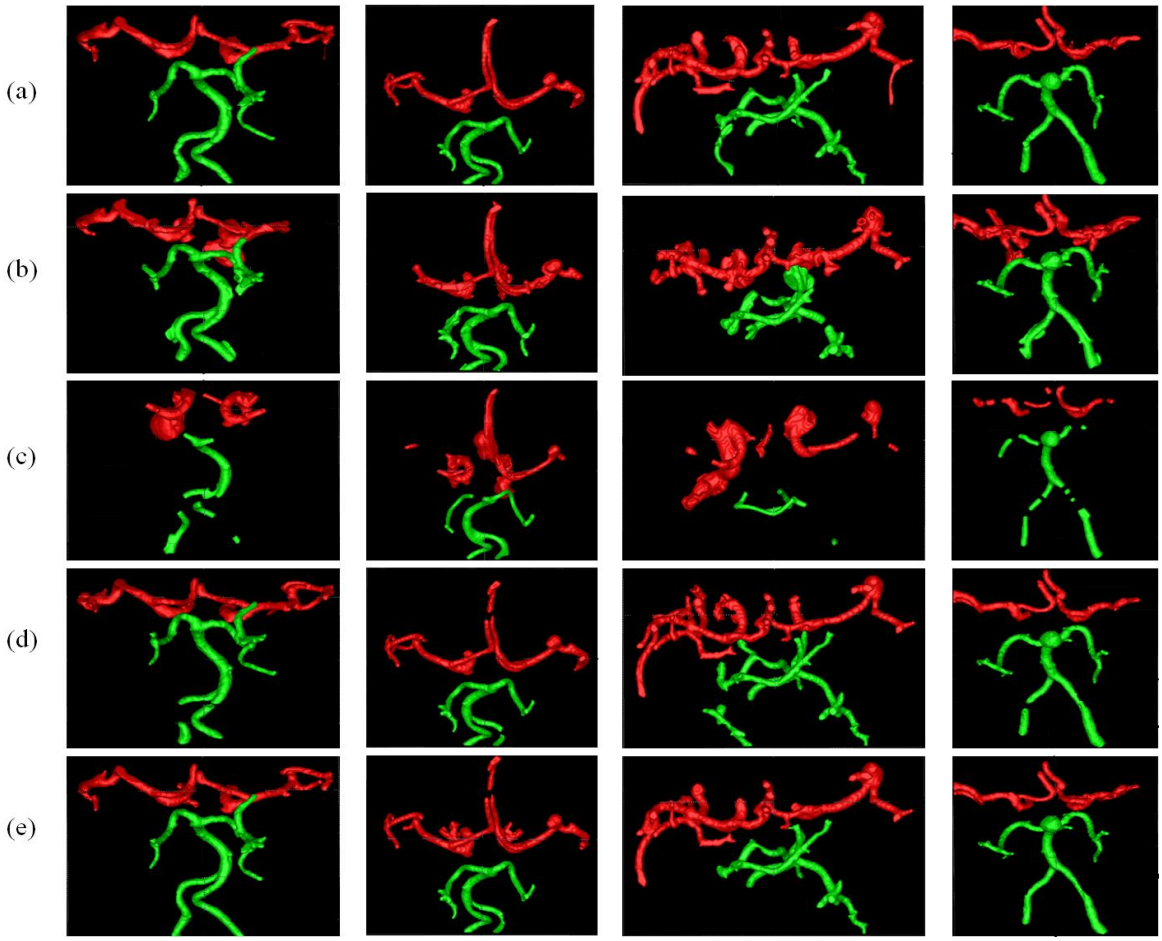

Fig. 7. (a) Ground-truth of dataset 1, 3, 4 and 5. (b) and (c) are segmentation results using region competition and geodesic active contours with optimized configurations, respectively. (d) and (e) are segmentation results based on adaptive GAC (single) and adaptive GAC (iterative), respectively. Red color denotes anterior cerebral circulation arteries and green color denotes posterior cerebral circulation arteries.

[5] S.C. Zhu, A. Yullie. Region Competition:Unifying Snakes, Region Growing, and Bayes/MDL for Multiband Image Segmentation. *IEEE Trans. Pattern Anal. Mach. Intell*. 1996. 18(9), 884-900.

[6] D. Nain, A.J.Yezzi, G. Turk. Vessel segmentation using a shape driven flow. *In Proc. of Med. Image Comput. Assist. Interv*. 2004. pp. 51‐59.

[7] Lesage, E.D. Angelini, I. Bloch, G. Funka-Lea. A Review of 3D Vessel Lumen Segmentation Techniques: Models, Features and Extraction Schemes. 2009. *Med. Image Anal.*. 13(2009) 819-845.

[8] A.F. Frangi, W.J. Niessen, K.L. Vincken, M.A. Viergever. Multiscale vessel enhancement filtering. *In Proc. of Med. Image Comput. Assist. Interv.* 1998. vol. 1496, pp. 130‐137.

[9] M. Hernandez, A. F. Frangi. Non-Parametric Geodesic Active Regions: Method and Evaluation for Cerebral Anerysm Segmentation in 3DRA and CTA. 2007. Med. Image. Anal. 11(2007) 224-241.

[10] S. Ali, A. Madabhushi. An Integrated Region-, Boundary-, Shape-Based Active Contour for Multiple Object Overlap Resolution in Histological Imagery. *IEEE Trans. on Med. Imaging*. 2012. Vol. 31, no. 7, July 2012.

[11] A. Lauric, E. Miller, S. Frishen, A. M. Malek. Automated Detection of Intracranial Aneurysms based on Parent Vessel 3D Analysis. 2010. *Med. Image. Anal.* 14(2010) 149-159.

[12] P. Yan, A.A. Kassim. Segmentation of Volumetric MRA Images by using Capillary Active Contour. 2006. *Med. Image Anal.* 10 (3), 317–329.

[13] M. Hernandez, A.F. Frangi. Brain aneurysm segmentation in CTA and 3DRA using geodesic active regions based on second order prototype features and non-parametric density estimation. *In Proc. of SPIE Medical Imaging* 2005: *Physiology, Function, and Structure from Medical Images*, vol. 5747, pp. 514–525.

[14] M. Rochery, I. Jermyn, J. Zerubia. Higher order active contours. *Int. J. Comput. Vision*. 2006. 69 (1), 27‐42. D.

[15] A. Vasilevskiy, K. Siddiqi. Flux maximizing geometric flows. *IEEE Trans. Pattern Anal. Mach. Intell*. 2002. 24 (12), 1565‐1578.

[16] M. Law, A. Chung. Three Dimensional Curvilinear Structure Detection using Optimally Oriented Flux. *In Proc. of Eur. Conf. Comput. Vision*. 2008. pp. 368‐382.

[17] M. Law, A. Chung. Efficient Implementation for Spherical Flux Computation and Its Application to Vascular Segmentation. *IEEE Trans. on Image Processing*. 2009. 18 (3), 596‐612.

[18] C. Bauer, H. Bischof. A novel approach for detection of tubular objects and its application to medical image analysis. *In Proc. DAGM Symp. Pattern Recognit*. 2008 pp. 163‐172.

[19] ITK.http://www.itk.org/.